Available online at www.sciencedirect.com
ScienceDirect
Diamond & Related Materials 17 (2008) 105–117
DIAMOND AND RELATED MATERIALS
www.elsevier.com/locate/diamond

Raman and conductivity studies of boron-doped microcrystalline diamond, facetted nanocrystalline diamond and cauliflower diamond films

P.W. May [a,*], W.J. Ludlow [a], M. Hannaway [a], P.J. Heard [b], J.A. Smith [a], K.N. Rosser [a]

[a] School of Chemistry, University of Bristol, Bristol BS8 1TS, UK
[b] Interface Analysis Centre, University of Bristol, Oldbury House, 121 St Michael's Hill, Bristol BS2 8BS, UK

Received 9 July 2007; received in revised form 16 October 2007; accepted 1 November 2007
Available online 13 November 2007

Abstract

We present a large amount of data showing how the electrical conductivity and Raman spectra of boron-doped CVD diamond films vary as a function of both B content and film type — in particular, diamond crystallite size. Three types of film have been investigated: microcrystalline diamond (MCD), faceted nanocrystalline diamond (f-NCD) and 'cauliflower' diamond (c-NCD). For the same B content (measured by SIMS), the conductance of MCD films was much higher than those for the two types of smaller grained films. Multi-wavelength laser Raman spectroscopy showed that Fano interference effects were much reduced for the smaller grain-sized material. The position of the Lorentzian contribution to the 500 cm^{-1} Raman feature was used to estimate the B content in each type of film, and compared to the value measured using SIMS. We found that the Raman method overestimated the concentration of B by a factor of ~5 for the f-NCD and c-NCD films, although it remains reasonably accurate for MCD films. The shortfall may be explained if only a small fraction of the B found in the small-grained films is being incorporated into substitutional sites. We conclude that in diamond films with a high concentration of grain boundaries, the majority of the B (80% in some cases) must be present at sites that do not contribute to the continuum of electronic states that give rise to metallic conductivity and the Fano effects. Such sites may include (a) interstitials, (b) the surface of the crystallites, or (c) bonded within the non-diamond carbon impurities present at the grain boundaries. This suggests that heavy doping of nanograined diamond films will give rise to a material with many different conducting regions, and possibly different conducting pathways and mechanisms.

Keywords: Laser Raman spectroscopy; CVD diamond; nanodiamond; Cauliflower diamond; Boron doping

1. Introduction

Diamond films produced by chemical vapour deposition (CVD) can be doped with boron to produce a p-type semiconducting material with electrical conductivity that ranges from insulating to metallic, depending upon the doping level [1]. The boron dopant atoms act as electron acceptors, and form a band located ~0.35 eV above the valence band edge. At low temperatures or at boron concentrations $<10^{17}$ cm^{-3} conduction occurs through holes in the valence band contributed by ionised substitutional B. At higher doping levels, conduction occurs by nearest-neighbour and variable range hopping of holes between ionised B sites [2], accompanied by a drop in mobility [3]. At very high doping levels, an impurity band is formed, giving rise to metal-like conductivity.

A complication is that polycrystalline boron-doped CVD diamond films possess grain boundaries containing a small-volume fraction of non-diamond carbon impurities. Consequently, the electrical conductivity of the film is a complicated function of the combined effects of the boron-doping level, the grain boundaries, and the impurities. As the grain size in the films becomes smaller, *i.e.* from microcrystalline diamond (MCD) to nanocrystalline diamond (NCD), the relative importance of these grain boundaries increases. As a result, most reports concerning B-doped diamond, both fundamental science-based and applications-led, have concentrated upon epitaxially-grown diamond or MCD films. There have been relatively few studies concerning B-doped NCD films, with the majority concerning their applications for electrochemical

* Corresponding author.
E-mail address: paul.may@bris.ac.uk (P.W. May).

0925-9635/$ - see front matter © 2007 Elsevier B.V. All rights reserved.
doi:10.1016/j.diamond.2007.11.005

electrodes [4] or other devices [5,6]. However, a recent theoretical study by Barnard and Sternberg [7] predicted that boron is likely to be positioned at the surface of isolated nanoparticles and at the grain boundaries in NCD films.

Unfortunately there is no rigorous definition for NCD in the literature, and the only agreed property is that the films have grain sizes in the nm range, typically between 10–500 nm, although even the exact range is arguable. In fact, a number of films with quite distinct characteristics all come under the broad umbrella of NCD [8]. One type of NCD film is deposited if the deposition occurs with a very high initial nucleation density (*e.g.* by using nanodiamond grit for abrasion), followed by standard growth conditions [9]. These films exhibit columnar growth, just as for MCD, except with nano-sized crystallites. There is little or no re-nucleation, and the grain size, and hence roughness, increase with film thickness, so above a thickness of around 1μm, the film becomes microcrystalline. Thus, these NCD films can be considered as just smaller grained, facetted versions of MCD, and we shall refer to them as 'facetted NCD' (f-NCD).

However, this description is not appropriate for many other NCD films, which often contain a significant fraction of non-diamond material, and exhibit no faceting or evidence of columnar growth, even at thicknesses of several μm. Some NCD films have a rounded appearance and as a result, their morphology is often referred to as 'ballas' (meaning ball-like) or cauliflower-like [10,11]. We shall call these types of films 'cauliflower NCD' (c-NCD). Thicker c-NCD films can be grown with essentially flat surfaces with nm smoothness, and this allows them to be patterned with much higher resolution than MCD. Decreasing the diamond crystallite size below 10 nm produces what has come to be known as 'ultrananocrystalline' diamond (UNCD) films [12]. However, there are as yet no reports of successful B doping of UNCD [13]. In this paper we shall concentrate upon comparing the doping behaviour, electrical properties, and Raman characteristics of boron-doped MCD, f-NCD and c-NCD films.

Studies of the Raman spectra from B-doped diamond films have also been restricted almost exclusively to epitaxial or MCD films [14]. The diamond phonon observed at 1332 cm^{-1} is a symmetric Lorentzian at low boron concentration, but as the boron concentration increases above a threshold of $\sim 10^{20}$ cm^{-3} — corresponding to the onset of metallic conductivity — there is an abrupt and pronounced change toward an asymmetric Fano-like lineshape [15]. This asymmetry is caused by a quantum mechanical interference between the zone-centre Raman-active optical phonon and the continuum of electronic states induced by the presence of the dopant. The threshold for the appearance of the Fano-like lineshape was found to depend on the excitation laser wavelength [16]. The Raman peak also shifts to lower wavenumber with increased boron concentration, and is accompanied by a wide signal (300–1330 cm^{-1}) with structures around 500 and 1225 cm^{-1} (although these structures do not appear when using ultraviolet (244 cm^{-1}) excitation [17]). Such results were first reported for epitaxially-grown diamond [18,19] and then confirmed [15,20] for polycrystalline boron-doped films. Wang et al. [17] found that this shift in the peak position was also a function of excitation wavelength in the range 244–514 nm. The origin of the 500 and 1225 cm^{-1} peaks is uncertain, but their positions approximately agree with two maxima in the phonon density of states (PDOS). They may therefore be connected with a relaxation of the wavevector selection rules, and if so, they may well be associated with the actual boron incorporation in the lattice, rather than the hole concentration [21]. There is also evidence [22] that the 500 cm^{-1} peak originates from local vibrational modes of boron pairs [23], which cause some distortion in the diamond lattice around these isolated defects. Alternatively, peaks similar to these have been seen in the Raman spectra of nanocrystalline diamond films, and assigned to amorphous sp^3-bonded carbon [24].

For very heavy B doping, the Fano parameters saturate and it becomes difficult to discern the position of the zone-centre phonon, with the peaks at 500 and 1225 cm^{-1} dominating the spectrum. For these conditions, the 500 cm^{-1} peak can be fitted with a combination of Gaussian and Lorentzian line shapes. The wavenumber position, ω, of the Lorentzian component approximately obeys [21]:

$$[\mathrm{B}]/\mathrm{cm}^{-3} = 8.44 \times 10^{30} \exp\left(-0.048\omega\right) \quad (1)$$

where ω is in cm^{-1} and the boron content, [B], is in the range from 2×10^{20} to 1×10^{22} cm^{-3}.

Here, we present results for the Raman spectra of boron-doped MCD, f-NCD and c-NCD films, as a function of B content, using a range of excitation wavelengths from the ultraviolet to the infrared, and extend the findings reported in our preliminary letters paper [25].

2. Experimental

The three types of diamond film were all grown in a standard hot filament CVD reactor using CH_4/H_2 process gases at a pressure of 20 Torr. The substrate was undoped single crystal (100) Si, abraded ultrasonically before deposition using a slurry of 100 nm diamond grit in water. Rhenium was used for the filament material rather than tantalum since Re does not act as a sink for carbon or boron species, unlike Ta which can absorb significant amounts of B and C for many hours into the deposition run [26]. The filament temperature was kept constant at 2400 °C and monitored using a 2-colour optical pyrometer, and the substrate temperature was maintained at ~900 °C. Diborane (B_2H_6) gas diluted in H_2 was used as the source of B at concentrations between 10–12000 ppm with respect to CH_4. All three gases were metered into the chamber using mass flow controllers.

For MCD and f-NCD, a ratio of 1%CH_4/H_2 was used, whereas for c-NCD the methane concentration was increased to 5%. The only difference between MCD and f-NCD was that for f-NCD the ultrasonic abrasion was performed for much longer to ensure high nucleation density, and the film growth was stopped after 90 min to give a continuous film < 1 μm thick with small facetted grains. MCD and c-NCD films were grown for 8 h giving films ~4 μm thick. The various film morphologies

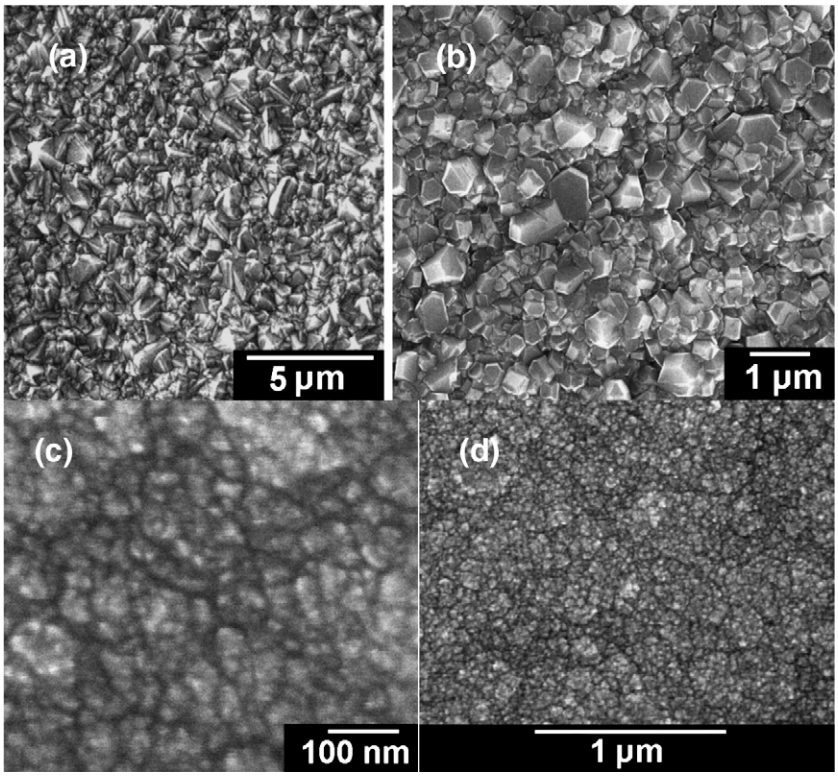

Fig. 1. Scanning electron micrographs of the surface of the three types of diamond film: (a) MCD, showing randomly-oriented grain sizes around 0.5–1 μm, (b) f-NCD, with grain sizes ~100–500 nm, and (c) and (d) c-NCD, with grains sizes 20–100 nm.

can be seen in Fig. 1. Undoped films were grown in a different but otherwise identical HF CVD reactor that had never used boron-containing gases. This is because B is known to diffuse into the sidewalls and components within a reactor, and then diffuse out again during later growth runs, inadvertently introducing B into the gas mixture and causing unwanted doping of any growing film. Use of a 'clean' B-free reactor removes this risk and allows films with zero B content to be deposited. Ironically, the fact that B diffuses out of the chamber walls of the reactor used for B doping during deposition, even when no B_2H_6 was added to the gas mixture, was useful to produce films with very low B doping, although controlling the doping levels in this case was hit-and-miss.

Electrical conductivity measurements were made by both two-point and four-point probe methods. In these, spring-loaded probes were pressed into contact with the surface of the film and the resistance measured over a distance of ~ 5 mm. Note that even though the four-point probe measurements supposedly remove most of the effects of contact resistance, these measurements were of the effective surface conductivity, and might not correspond to the bulk conductivity. The 4-point resistance measurements could, in principle, be converted to resistivity values in Ω per square, if the thickness of each of the films were known. However, since (a) the thickness varies from sample to sample, (b) there is quite a bit of uncertainty regarding what the true thickness is for very thin films, and (c) the conductivity is not uniform throughout the entire thickness of the film (the surface is likely to be more conducting than the bulk), this conversion would not yield accurate or useful values. Linear plots of current against applied voltage, passing through the origin, were obtained, showing that the contacts were Ohmic.

Boron content within the film was measured using secondary ion mass spectrometry (SIMS), with the B:C count ratio being calibrated with respect to those from two reference samples. The first reference was a single crystal diamond implanted with a known dosage of B, and therefore containing a known B content. The second reference was an undoped CVD diamond film

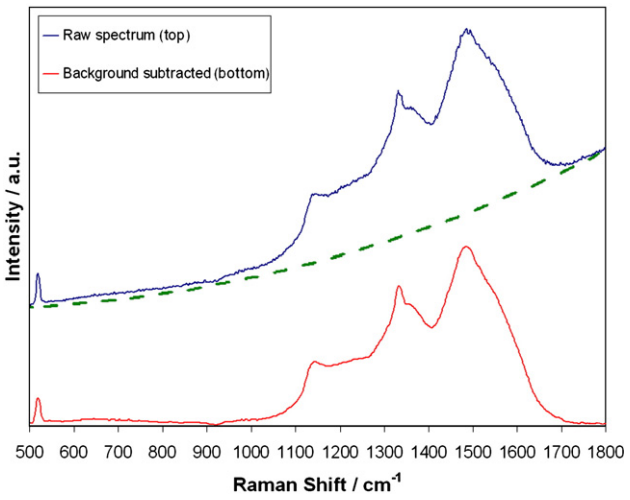

Fig. 2. An example of a PL background subtraction from the Raman spectrum of a very lightly doped f-NCD film viewed using 514 nm (green) excitation. The dashed line is the fitted PL background.

Table 1
B content as measured by SIMS, and as estimated from fitting the 500 cm^{-1} Raman peak using Eq. (1), plus 2-point and 4-point resistance measurements for the 3 types of films

	B content/cm^{-3} (SIMS)	B content/cm^{-3} (Raman fit)	2-point resistance/Ω	4-point resistance/Ω
MCD				
M1	0	–	4.8×10^{7}	7600
M2	2.4×10^{19}	–	1.6×10^{5}	1550
M3	7.5×10^{19}	–	8.1×10^{4}	500
M4	3.7×10^{20}	3.0×10^{20}	520	81
M5	*6.0×10^{20}*	4.0×10^{20}	200	52
M6	1.5×10^{21}	7.2×10^{20}	20	20
M7	*2.3×10^{21}*	1.4×10^{21}	6	9
f-NCD				
F1	0	–	1×10^{7}	9.0×10^{4}
F2	1.5×10^{20}	–	23,000	3800
F3	1.4×10^{20}	–	18,000	3700
F4	*5.0×10^{20}*	–	10,000	1000
F5	1.3×10^{21}	2.6×10^{20}	1300	121
F6	2.4×10^{21}	3.0×10^{20}	400	95
F7	2.8×10^{21}	8.7×10^{20}	230	67
c-NCD				
C1	0	–	2×10^{8}	1×10^{7}
C2	6.0×10^{18}	–	1×10^{7}	5×10^{6}
C3	6.1×10^{20}	–	22,000	6480
C4	1.1×10^{21}	3.4×10^{20}	2500	294
C5	2.9×10^{21}	4.5×10^{20}	360	66
C6	6.1×10^{21}	9.6×10^{20}	60	43

The italicised values for SIMS B content for M5, M7 and F4 indicates that these were not measured directly, but were interpolated from a plot (Fig. 4) of four-point resistance against B content for the other films in that series.

with zero B content, providing the background count level for B.

Laser Raman spectra were obtained at room temperature using a Renishaw 2000 spectrometer and a range of excitation wavelengths and lasers: UV 325 nm (HeCd), blue 488 nm (Ar^{+}), green 514 nm (Ar^{+}), red 625 nm HeNe, IR 785 nm (IR diode), and far IR 830 nm (IR diode). Undoped or lightly doped films often exhibited a large rising or falling photoluminescent (PL) background upon which the much smaller Raman features would sit. This PL background would decrease markedly with even trace amounts of B doping, and for B contents $>5\times10^{18}$ cm^{-3} it disappeared altogether giving a flat baseline. The reason for this may be that the B is compensating the nitrogen-related defects within the diamond that give rise to the majority of the PL. Therefore, in order to see the small Raman features more clearly, and to reproduce the spectra from the undoped films on the same scale as the doped ones, it was useful to subtract this PL background where necessary. This was done

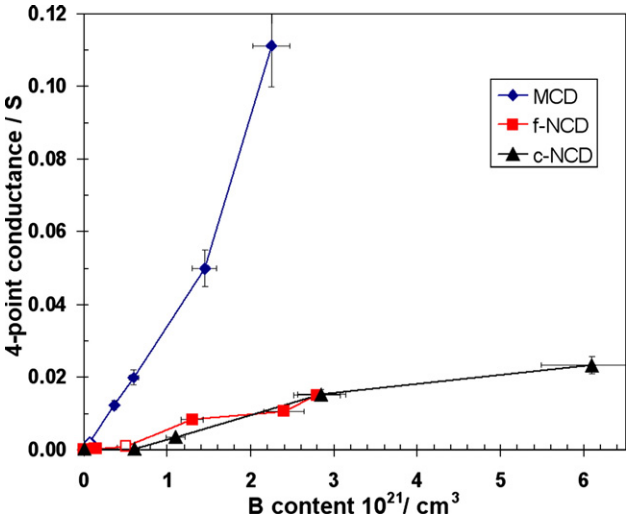

Fig. 4. B content plotted against measured 4-point conductance (1/resistance) for the 3 types of films. Filled points are measured SIMS values of B content, the hollow points are estimated values of B content based on inter/extrapolation of the trends from the other points. B content values are estimated to be accurate to ±10%, as shown by error bars.

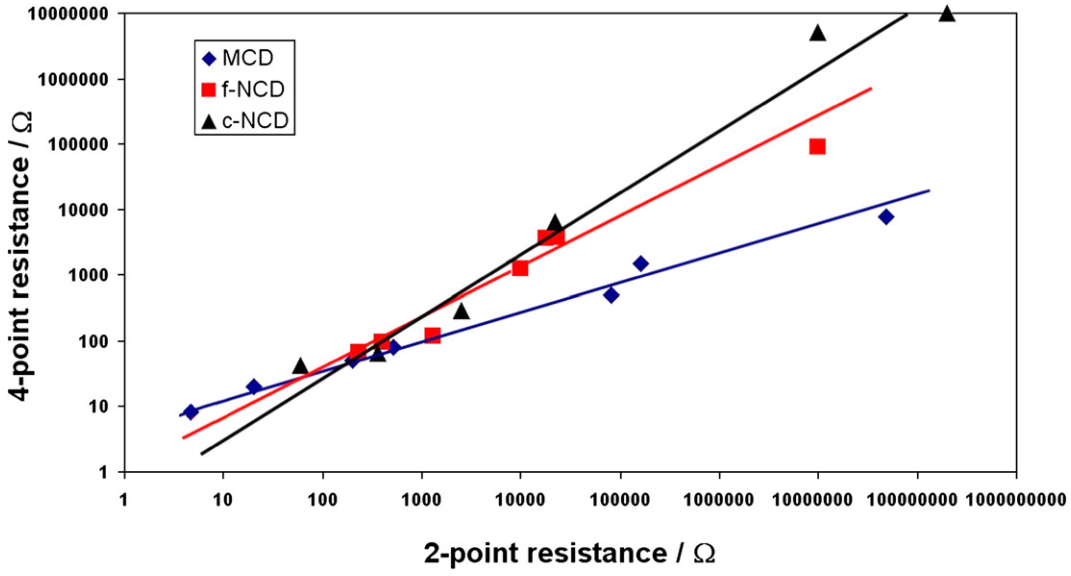

Fig. 3. Plot of 2-point resistance against 4-point resistance for the 3 types of film. Linear lines of best fit have been added to aid the eye.

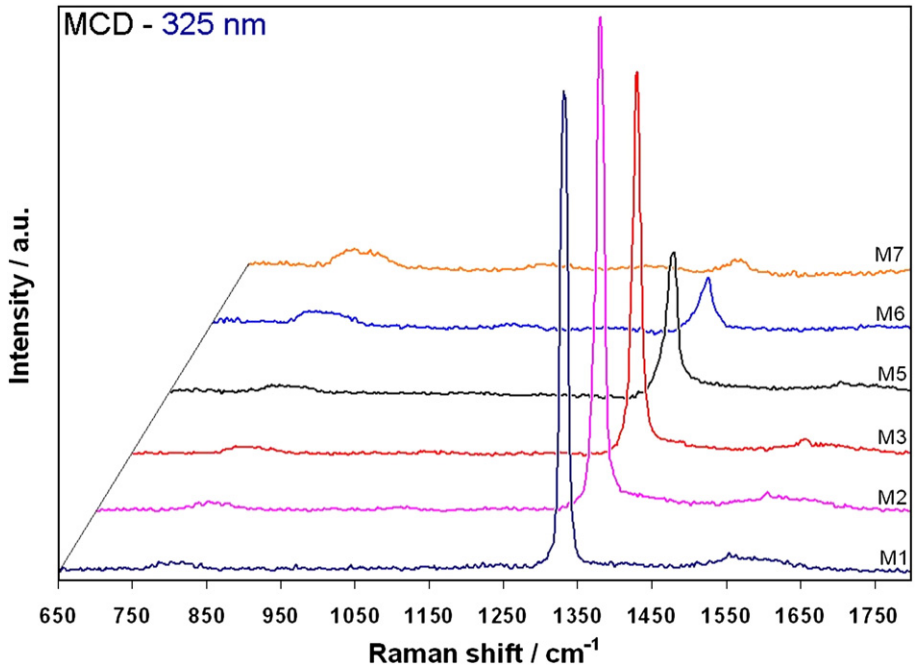

Fig. 5. Raman spectra for the different boron-doped MCD films using UV (325 nm) excitation. The films increase in B content from M1 (undoped) to M7 heavily doped, with the details given in Table 1. The spectra have been offset vertically and by 50 cm^{-1} horizontally from each other for clarity. Features below 650 nm were not visible due to the cut-off filter used to remove the UV laser line.

by fitting a polynomial curve to the background, and then subtracting this to obtain a processed spectrum, as illustrated in Fig. 2. With increasing B content, the films became visibly darker and often looked bluish, and the Raman signals became correspondingly less intense. Longer accumulation times were required to obtain reasonable signal:noise levels in these samples.

In those samples where the 500 cm^{-1} band was discernible (*i.e.* the more heavily doped samples), the band was fitted to a Gaussian curve centred ~500–550 cm^{-1} and a Lorentzian curve

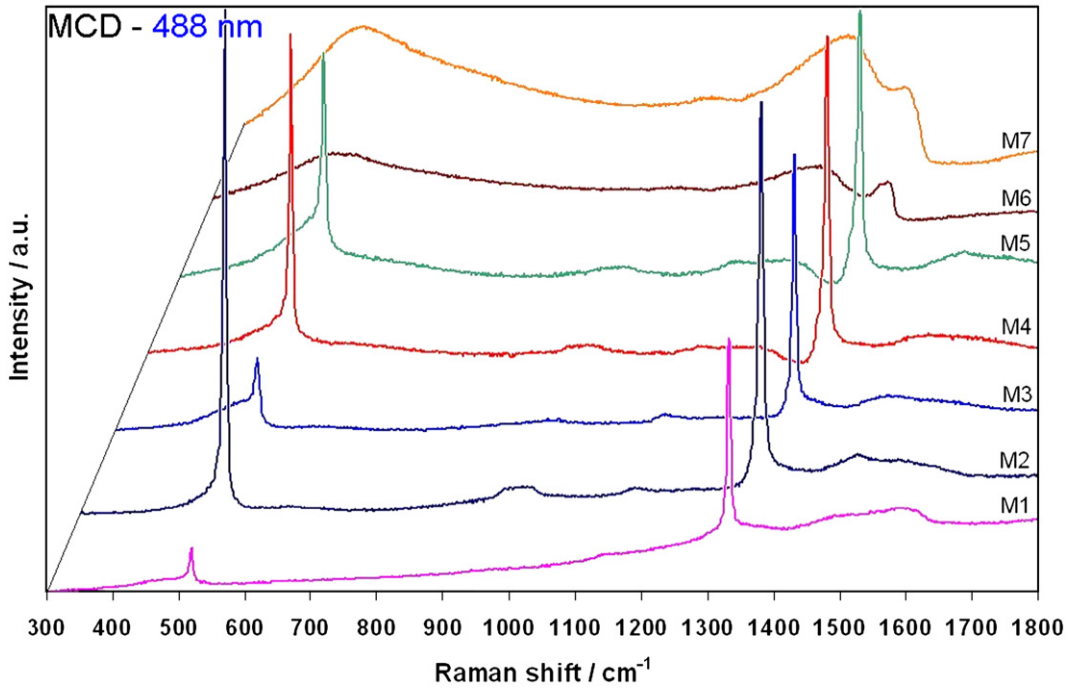

Fig. 6. Raman spectra for the different boron-doped MCD films using blue (488 nm) excitation. The films increase in B content from M1 (undoped) to M7 heavily doped, with the details given in Table 1. The spectra have been offset vertically and by 50 cm^{-1} horizontally from each other for clarity. No PL backgrounds have been subtracted since only M1 showed any significant rising background and this was small enough to be neglected. M1 has been scaled down in intensity by a factor of 10 to facilitate comparison with the other spectra. The broad feature between 900–1000 cm^{-1} is the second order of the Si line from the substrate.

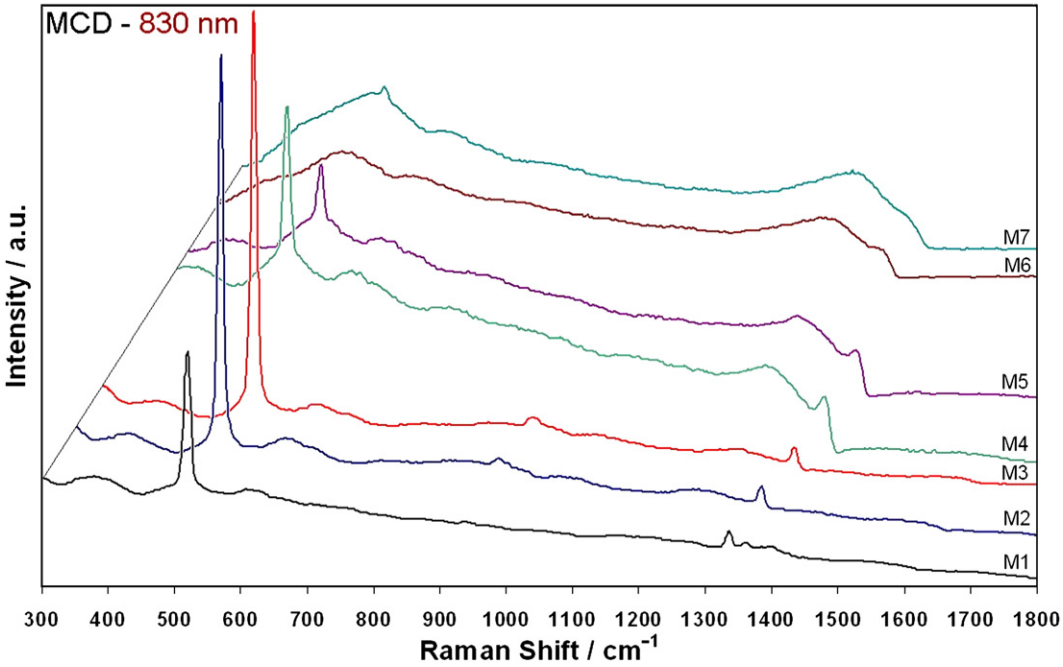

Fig. 7. Raman spectra for the different boron-doped MCD films using far IR (830 nm) excitation. The films increase in B content from M1 (undoped) to M7 heavily doped, with the details given in Table 1. The spectra have been offset vertically and by 50 cm^{-1} horizontally from each other for clarity, with no PL background subtraction. The intensities in the spectrum for M1 have been scaled down by a factor of 5 to facilitate comparison between spectra.

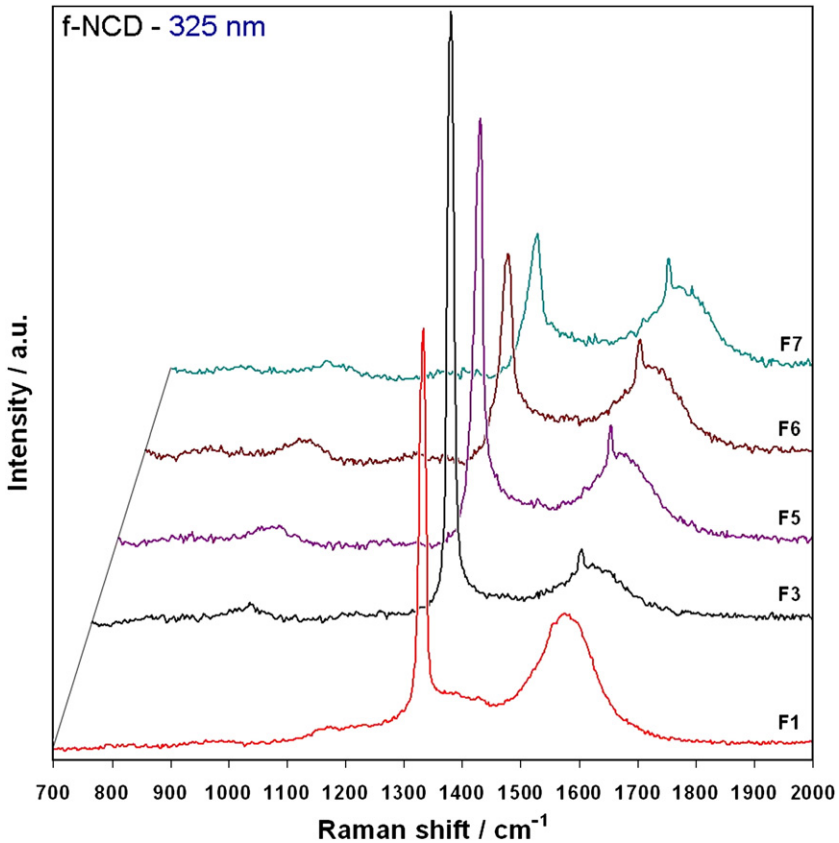

Fig. 8. Raman spectra for the different boron-doped f-NCD films using UV (325 nm) excitation. The films increase in B content from F1 (undoped) to F7 heavily doped, with the details given in Table 1. The spectra have been offset vertically and by 50 cm^{-1} horizontally from each other for clarity, with no PL background subtraction. The intensities in the spectrum for F1 have been scaled down by a factor of 2 to facilitate comparison between spectra.

centred ~460–505 cm^{-1} following the procedure outlined in Ref. [21]. Using the relationship between the B content and the wavenumber of the Lorentzian component of the 500 cm^{-1} band (Eq. (1)), it was possible to estimate the doping levels in these films, with which to compare the values from SIMS.

3. Results

3.1. Electrical results

The doping levels and resistance values for the 3 sets of films are given in Table 1. The undoped MCD and f-NCD films had 2-point resistance values in the tens of MΩ, whereas the undoped c-NCD films were much more resistive, having resistance values >100 MΩ. These values reduced to only a few Ω (*i.e.* metallic conductivity) for all types of films when they were highly doped — a range of 7–8 orders of magnitude in conductivity. The 4-point resistance measurements are substantially lower than the 2-point measurements (see Fig. 3), showing that the contact resistance for mechanical spring-loaded contacts is significant. As Fig. 3 shows, on a log–log plot the measured 2-point and 4-point values show a roughly linear dependency, with the gradients of the linear best fit lines increasing as the crystallite size decreases.

The values of the boron content in the films are plotted against 4-point conductance (=1/resistance) in Fig. 4. The trends are roughly linear for all three film types, but the conductance of the MCD films is higher than those for the other two films, for the same B doping. This suggests that the doping efficiency for MCD films is greater than for the other two types, and this might be explained if a greater proportion of the incorporated B atoms were contributing to doping in MCD. In f-NCD and c-NCD films, the reduced doping efficiency suggests that a significant amount of the B is being incorporated in positions (such as at the grain boundaries), which do not improve the conductivity to the same extent as doping the crystallites themselves. The incorporation of B at the grain boundary may still affect the overall film conductivity, since 'grain boundary doping' may provide alternative conduction pathways that compete with the through-grain conduction. This will be explored following more detailed conductivity measurements to appear in a subsequent paper.

3.2. Laser Raman spectra

Although laser Raman spectra were obtained for 6 different laser wavelengths, only those spectra which show substantial differences from each other will be presented here.

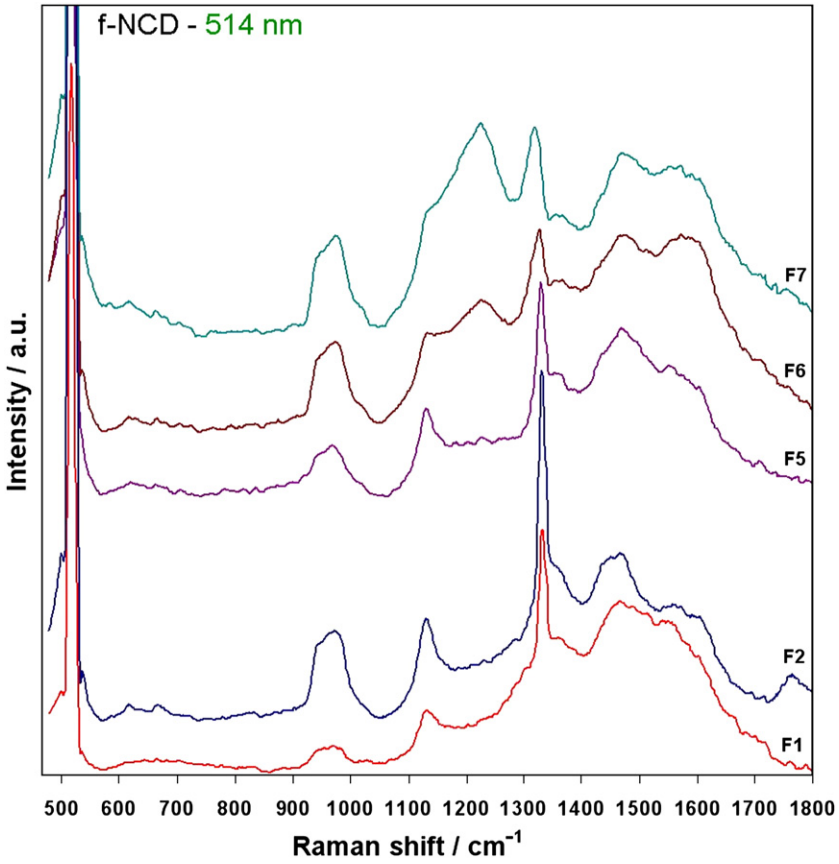

Fig. 9. Raman spectra for the different boron-doped f-NCD films using green (514 nm) excitation. The films increase in B content from F1 (undoped) to F7 heavily doped, with the details given in Table 1. The spectra have been offset vertically from each other for clarity, with PL background subtraction applied to all of them to produce a flat baseline. The intensities in the spectrum for F1 have been scaled down by a factor of 2 to facilitate comparison between spectra. The Si line at 520 cm^{-1} dominates these spectra, and when the spectra are magnified to show the important details of the diamond peaks, this Si line goes off scale. The large feature around 900–1000 cm^{-1} is the second order from this intense Si line.

3.2.1. MCD films

The Raman spectra of the MCD films excited in the UV, green and far IR are shown in Figs. 5–7. In the UV spectrum (Fig. 5), the diamond peak decreases in intensity and broadens with increasing B content. The line also exhibits an asymmetric Fano lineshape for the samples doped higher than M2 ([B] $\sim 2.4\times10^{19}$ cm^3), which is at a smaller doping level than usually observed in epitaxial diamond films [15]. There is a small G band present with a peak at ~1580 cm^{-1} due to crystalline graphite impurities. A new broad feature at ~800 cm^{-1} is apparent in all these films. Notably, the 1225 cm^{-1} peak is absent from the spectrum of even the most highly doped sample, as reported by Wang et al. [17].

The blue Raman spectra (Fig. 6) show trends similar to those observed previously by other groups [15,17,18]. Spectra obtained with green, red and IR excitation are not substantially different in character to Fig. 6 and so have not been shown here for brevity. In Fig. 6, the diamond peak shifts to lower wavenumber with increasing B content, and the lineshape becomes asymmetric due to Fano interference above a B concentration of $\sim 3.7\times10^{20}$ cm^3 (sample M4). The broad 1225 cm^{-1} feature increases with B concentration and dominates the spectrum at high B content. The G band is evident at low B concentrations, but is not very intense, and at higher B concentrations, as the film achieves metallic conductivity (M6 and M7), it disappears. This does not imply that there is less graphite in these films, only that the G band signal is hidden beneath those from the other nearby features. The peak at ~1150 cm^{-1}, which is normally characteristic of nanophase diamond but is probably due to sp^2 C species at grain boundaries [27], is weakly present for the undoped film, but increases with B concentration, suggesting that B promotes the incorporation of sp^2 carbon species, probably at grain boundaries. At even higher B concentrations, this peak is hidden beneath the 1225 cm^{-1} peak. The Si line at 520 cm^{-1} generally decreases in intensity with B concentration as the films become darker and less transmitting to the blue laser light, however there is a fluctuation in the trend due to variations in the laser focusing position. The broad feature centred at ~500 cm^{-1} becomes more intense with increasing B, and shifts to higher wavenumber (as mentioned by ref.[16]), eventually swamping the Si peak.

The far IR spectra (Fig. 7) show similar features to the blue ones, with the diamond peak shifting to lower wavenumber and attaining a Fano lineshape with increasing B content. The 1225 cm^{-1} feature has become much more intense at lower B concentrations, and even by sample M4 ([B] $\sim 3.7\times10^{20}$ cm^3) dominates the high wavenumber region of the spectrum. The 500 cm^{-1} feature increases with B content, and a new feature at ~600 cm^{-1}, which is weakly present in the spectrum from the undoped sample, also increases with B content.

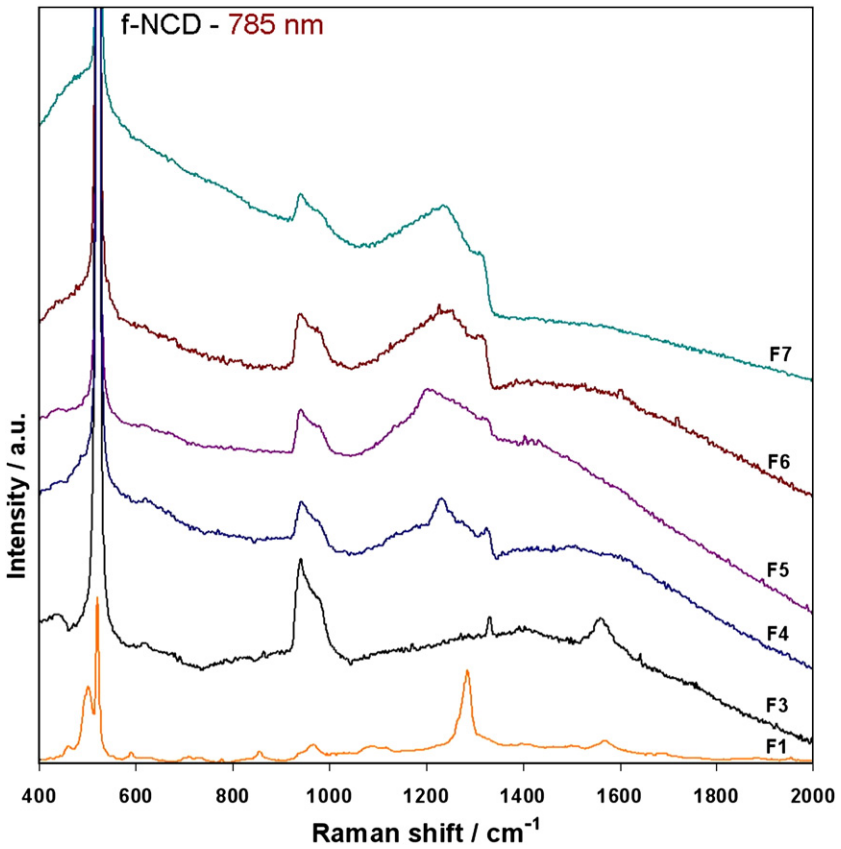

Fig. 10. Raman spectra for the different boron-doped f-NCD films using IR (785 nm) excitation. The films increase in B content from F1 (undoped) to F7 heavily doped, with the details given in Table 1. The spectra have been offset vertically from each other for clarity, with PL background subtraction applied to F1 only. The large feature around 900–1000 cm^{-1} is the second order from the Si line.

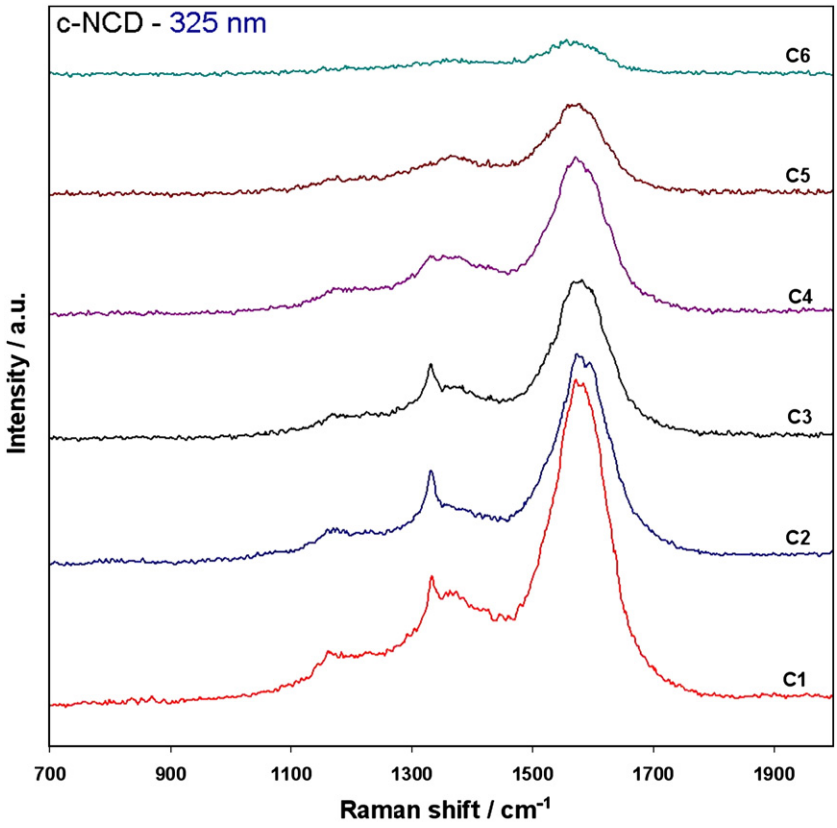

Fig. 11. Raman spectra for the different boron-doped c-NCD films using UV (325 nm) excitation. The films increase in B content from C1 (undoped) to C6 heavily doped, with the details given in Table 1. The spectra have been offset vertically from each other for clarity, with no PL background subtraction.

3.2.2. f-NCD films

The Raman spectra of the f-NCD films excited in the UV, green and IR are shown in Figs. 8, 9 and 10. The UV spectra (Fig. 8) are similar in appearance and trends to those for the MCD films (Fig. 5), except that the G band is more prominent due to the increased sp^2 carbon content at the grain boundaries. There is a peak at 1580 cm^{-1} due to crystalline graphite, which becomes more prominent at higher B content. This suggests that addition of large amounts of B is accompanied by an increasing graphitisation at the grain boundaries, although SEM analysis showed that the size of the grains and morphology did not appear to change appreciably — remaining the same as that in Fig. 1(b) for all B concentrations.

The green spectra (Fig. 9) show the diamond line, which again became broader, less intense, and shifted to lower wavenumber with increasing B content. The 1150 cm^{-1} feature is much more prominent than it was in the spectra for MCD films (Fig. 6), which is consistent with it being due to polymeric sp^2 C species at the grain boundaries [27]. The feature does not shift position with B concentration. A companion peak to this, a broad band centred ~1450 cm^{-1}, and the D peak (~1380 cm^{-1}) are also observed in all spectra, and also do not appear to change with B doping level. The G band appears to have more structure than before, with at least two broad features centred ~1560 and 1600 cm^{-1} contributing to the overall shape of the feature. The 1225 cm^{-1} feature that dominated the spectra of the highly doped MCD films is still present, but is much less dominant for these f-NCD films, and even at the highest doping level (F7) the diamond peak and the 1225 cm^{-1} peak remain separate and distinguishable. The broad feature at ~500 cm^{-1} is also less intense than for the MCD films, and is now almost entirely hidden beneath the intense Si line.

The IR spectra (Fig. 10) show a gradual evolution with B concentration, except for F1 which at first glance appears anomalous, since it has a large number of unusual peaks that do not appear in the same place as the other samples. In particular, in the F1 spectrum there are peaks at 500 cm^{-1} (even though there is no B present), several distinct peaks between 550 and 900 cm^{-1}, an intense peak at ~1280 cm^{-1}, no diamond peak, and a feature (presumably the G band) at ~1580 cm^{-1}. This spectrum also had a very intense PL background, which has been subtracted for the purposes of comparison with the other spectra. Unusual features such as these have been noted before in the IR Raman of thin diamond films [28] grown on Si. Recent work by ourselves [29] has shown them to be dependent upon film thickness, and they disappear above a thickness of ~30 μm, suggesting that the IR laser is probing sp^2 C structures at the diamond/Si interface. With even trace amounts of B doping (sample F3), the film becomes sufficiently opaque that the PL background reduces in intensity significantly making a PL background subtraction unnecessary. At the same time, most of

these peaks disappear, and we now only observe the expected peaks due to Si (520 cm^{-1}), diamond (1332cm^{-1}), and the G band 1580 cm^{-1}. With increasing B content, as before, the 1225 cm^{-1} peak grows in intensity, whilst the diamond peak weakens, broadens and shifts slightly to lower wavenumber. The 500 cm^{-1} peak also appears, but only for the highest B concentrations.

3.2.3. c-NCD films

The Raman spectra of the f-NCD films excited in the UV, green and IR are shown in Figs. 11–13. The UV spectra (Fig. 11) are similar in appearance and exhibit similar trends to those for the f-NCD (Fig. 8) and MCD films (Fig. 5), although the diamond peak is now much reduced in intensity compared to the strong D and G peaks. The 1170 cm^{-1} peak is also relatively prominent. These observations indicate that the amount of non-diamond carbon present in these cauliflower films is significantly higher than for the other two types of films, which is consistent with their smaller grain size and higher grain boundary density. However, the peak at 1580 cm^{-1} from crystalline graphite, which appeared strongly in the more highly doped f-NCD UV spectra, does not appear in the spectra for c-NCD. This suggests that the formation of detectable quantities of crystalline graphite requires both high B doping and the presence of crystal facets, otherwise the non-diamond carbon instead occurs as other phases, such as amorphous carbon. With increasing B content, the diamond peak and the 1170 cm^{-1} peak reduce in intensity compared to the broad D and G bands, possibly indicating that the crystallite size is decreasing (although this couldn't be discerned by SEM analysis) and that the films are becoming dominated by amorphous, rather than crystalline material. Indeed, the spectrum for sample C6 more closely resembles that from a diamondlike carbon film, than a diamond film.

The green spectra all exhibited extremely strong PL backgrounds, which have been subtracted in Fig. 12 to allow comparison between the important features of the spectra. The diamond peak is again less prominent, whereas the 1170 cm^{-1} peak is now relatively intense and its companion peak (~1450 cm^{-1}) is now stronger than the D and G bands. For higher B concentrations, the G band becomes more structured, with two peaks appearing at ~1560 and 1600 cm^{-1}, similar to the observations for f-NCD films. With increasing B content, the 1225 cm^{-1} peak intensity increases, eventually hiding the weaker 1170 cm^{-1} and diamond peaks. The diamond peak itself becomes wider and smaller with increasing B content, and only

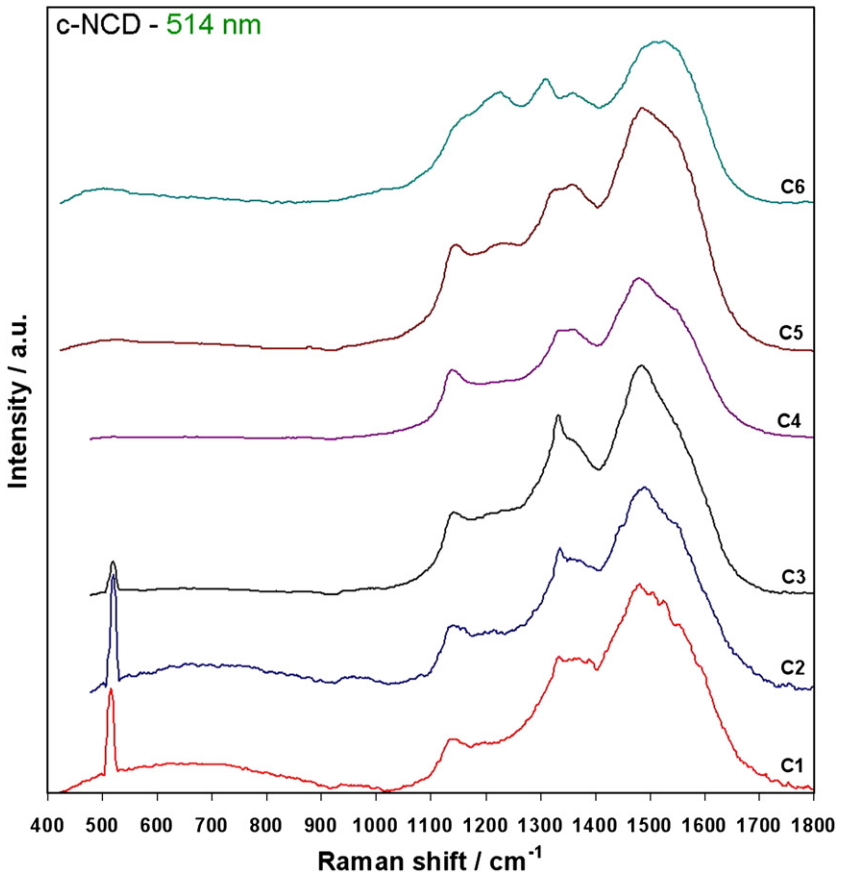

Fig. 12. Raman spectra for the different boron-doped c-NCD films using green (514 nm) excitation. The films increase in B content from C1 (undoped) to C6 heavily doped, with the details given in Table 1. The spectra have been offset vertically from each other for clarity, with PL background subtraction applied to all of them to produce a flat baseline. The PL background levels for C1 and C2 were respectively ~10× and ~5× those of the more heavily doped films, and uncertainties in the background subtraction procedure may have artificially produced the broad features seen between 400–900 cm^{-1} in the spectra of C1 and C2.

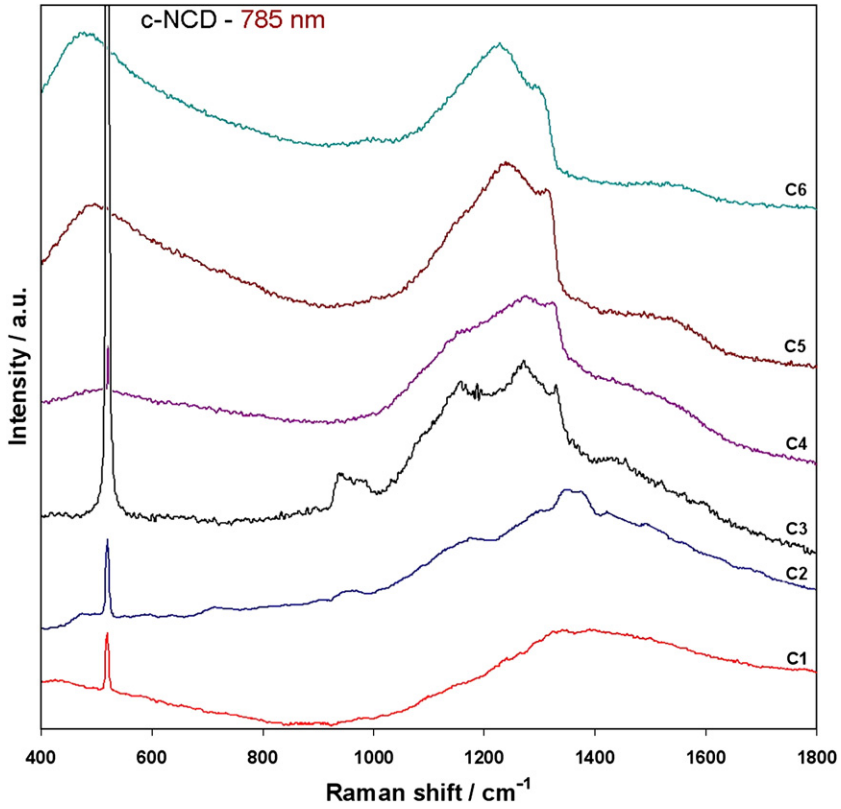

Fig. 13. Raman spectra for the different boron-doped c-NCD films using IR (785 nm) excitation. The films increase in B content from C1 (undoped) to C6 heavily doped, with the details given in Table 1. The spectra have been offset vertically from each other for clarity, with no PL background subtraction. The intensities in the spectra for C1 and C2 have been scaled down by a factor of 10 to facilitate comparison between spectra. The large feature around 900–1000 cm^{-1} is the second order from the Si line.

shifts a small amount to lower wavelength. The Si peak also decreases with B content, until it, too, is hidden by the more intense 500 cm^{-1} band.

The IR spectra (Fig. 13) show very few features for low B content films, with just a Si peak and a broad PL background centred around 1330 cm^{-1}. However, with increasing B, the PL background diminishes allowing more features, such as the diamond line, the 1170 cm^{-1} peak, and the G band to become apparent. With further increases in B, the 1225 cm^{-1} peak grows in intensity and shifts to higher wavenumber, while the diamond line attains the Fano lineshape. At the same time, the Si line disappears as the 500 cm^{-1} feature becomes much more intense.

3.2.4. Multi-wavelength Raman spectra of the heaviest doped films

It is worthwhile comparing directly the Raman spectra of the heaviest B-doped films as a function of excitation wavelength, and this is shown in Fig. 14. For the heavily B-doped MCD film (sample M7), the UV spectrum is clearly different to the others, with features at 800 and 1050 cm^{-1}, as well as the graphite peak at 1550 cm^{-1} appearing here and not in the other spectra. For all the other spectra there is a clear trend with the 1225 cm^{-1} peak gradually shifting to higher wavenumber, whilst the diamond peak shifts to lower wavenumber and broadens. The relative intensity of the 500 cm^{-1} peak increases with increasing laser wavelength. This is also true for the f-NCD spectra (sample F7), with the diamond peak well resolved in the UV spectrum, but having merged into the large 1225 cm^{-1} peak in the IR spectrum. For the c-NCD spectra (sample C6), the diamond peak is not well resolved in either the UV or the green spectra, and is only really apparent as a shoulder on the 1225 cm^{-1} peak in the IR spectrum.

Fig. 15 shows the position of the diamond peak for the heaviest doped samples as a function of excitation wavelength. For the heavily B-doped MCD sample, the peak position shifts to lower wavenumber with increasing laser wavelength, as noted by Wang et al. [17]. For the f-NCD films, this shift is less severe, and for the c-NCD films there is no apparent shift, within the resolution of the Raman spectrometer. This suggests that the Fano-type interference of the diamond line is a function of crystallite size, and for nm-sized crystals the effect is drastically reduced.

3.2.5. Estimation of B content from the 500 cm^{-1} Raman line

Table 1 shows the values for B concentration for the heavier doped films estimated from the Raman fit of the 500 cm^{-1} peak and using Eq. (1). The values for the MCD films are all within a factor of 2 of those measured by SIMS, showing that for MCD films, Eq. (1) is quite accurate. However, for the f-NCD films the estimated values are much less accurate, underestimating the SIMS values by factors of between 3 and 10. The same is true

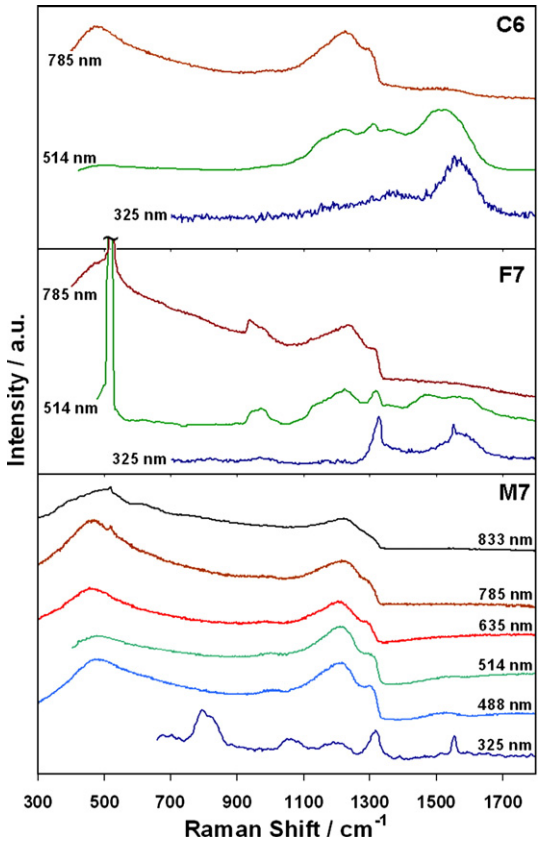

Fig. 14. Raman spectra for the most heavily B-doped of the three types of film, M7, F7 and C6 (details in Table 1), for a range of different laser excitation wavelengths from the UV to the far IR. The spectra have been offset vertically from each other for clarity, with no PL background subtraction (except for F7, green), and have been scaled in intensity to allow ease of comparison. The large Si peaks at 520 cm^{-1} in F7 (green and IR) have been truncated for clarity.

for the c-NCD films, where the values underestimate those from SIMS by factors of between 3 and 6. The difference arises since SIMS counts *all* the B present in the film, whereas the Raman method only counts those boron atoms which directly affect the 500 cm^{-1} band.

4. Conclusions

We have presented a large amount of data showing how the conductivity and Raman spectra of B-doped diamond films vary as a function of both B content and film type — in particular, diamond crystallite size. The different wavelength excitations provide different information about the films, and used together, they form a powerful diagnostic tool. UV (325 nm) excitation is probably the least useful for these B-doped films, since the Fano resonance and the 500 and 1225 cm^{-1} peaks do not appear in these spectra. However, it does allow the 1170 cm^{1} peak to be seen, giving information about the sp^2 content at the grain boundaries. IR (725 nm) excitation does provide information from the Fano shifts and 500 and 1225 cm^{1} peaks, although at low B doping the spectra often have few distinct features, making films difficult to tell apart. Visible excitation (488 or 514 nm) seems to be the best for obtaining maximum information, since the Fano resonance is easily observed, the 500 and 1225 cm^{-1} peaks occur readily, and there are many distinct features in all the spectra with which to compare films. However, visible excitation suffers from a very strong PL background for undoped or very lightly doped samples, which should be subtracted before comparisons with other films can be made.

We found that the conductance of B-doped MCD films was much higher than those for the smaller grained films, for the same B content. We also found that the Fano interference effects were much reduced for the smaller grain-sized material, and that Eq. (1) overestimates the concentration of B in the films by a factor of ~5 for the f-NCD and c-NCD films, although it remains reasonably accurate for MCD films. Eq. (1) measures only those boron atoms which directly incorporate into the diamond lattice (and hence affect the position of the 500 cm^{-1} band). The shortfall between these values and the 'true' values measured by SIMS may be explained if only a small fraction of the B found in the small-grained films is being incorporated into substitutional sites. The majority of the B (80% in some cases) must be present at sites that do not contribute to the continuum of electronic states that give rise to metallic conductivity and the Fano effects. Such sites may include (a) interstitials, (b) the surface of the crystallites, or (c) bonded within the non-diamond carbon impurities present at the grain boundaries. This is consistent with the theoretical predictions [7] that B is likely to be preferentially located in or near grain boundaries. This suggests that heavy doping of nanograined diamond films will give rise to a material with many different conducting regions, and possibly different conducting pathways and mechanisms. Not only are the nanograins doped, possibly up to the point of metallic conductivity, but the surface layer of each grain may have a higher concentration of B, allowing conducting pathways around each grain. Furthermore, the amount of non-diamond carbon at the grain boundaries, specifically graphite, increases with B addition, giving yet another potential conduction route. And finally, the presence of B inside this graphitic impurity layer may provide yet another mechanism for electron transport. Nevertheless, despite the complexity of the

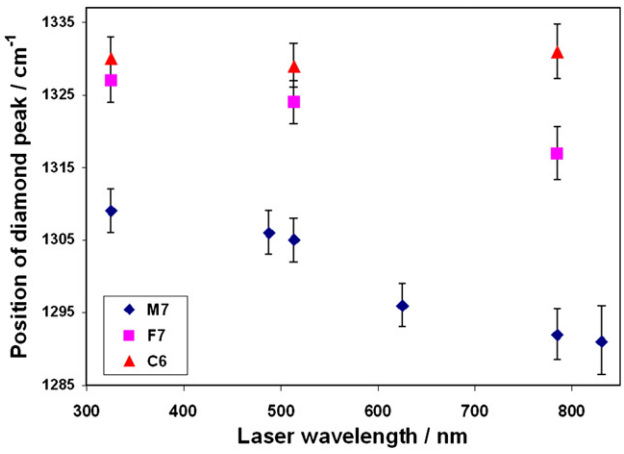

Fig. 15. The position of the diamond peak as a function of excitation wavelength for the three types of heavily B-doped diamond film.

underlying conduction mechanisms present in f-NCD and c-NCD films, they can be fabricated with controllable conductivities and nm-smooth surfaces, which might make them ideal candidates for use as an electronic material.

Acknowledgements

The authors would like to thank Jacob Filik, Martin Kubal & Tim Batten, and Keith Hallam & Diana Edwards for use of their far IR, blue, and red Raman systems, respectively, Jonathan Jones for the high resolution SEM photos, and Ulrika Dhaenens-Johansson of the University of Warwick for help with some of the Raman peak assignments.

References

[1] R. Kalish, Carbon 37 (1999) 781.
[2] B. Massarani, J.C. Bourgoin, R.M. Chrenko, Phys. Rev. B 17 (1978) 1758.
[3] K. Nishimura, K. Das, J.T. Glass, J. Appl. Phys. 69 (1991) 3142.
[4] Yu. V. Pleskov, Russ. J. Electrochem. 38 (2002) 1275.
[5] M. Willander, M. Friesel, Q.-ul. Wahab, B. Straumal, J. Mater. Sci: Maters in Electron. 17 (2006) 1.
[6] D.L. Dreifus, A. Collins, T. Humphreys, K. Das, P.E. Pehrsson (Eds.), Diamond for Electronic Applications, MRS Symp. Proc., vol 416, Materials Research Society, Pittsburgh, 1996.
[7] A.S. Barnard, M. Strernberg, J. Phys. Chem. B 110 (2006) 19307.
[8] P.W. May, Chemical vapour deposition — a route to microcrystalline, nanocrystalline, ultrananocrystalline and single crystal diamond films, Chapter in: Carbon Based Nanomaterials, A. Öchsner, W. Ahmed (Eds.) (Trans Tech, Switzerland, in press).
[9] O.A. Williams, M. Daenen, J. D'Haen, K. Haenen, J. Maes, V.V. Moshchalkov, M. Nesládek, D.M. Gruen, Diamond Relat. Maters. 15 (2006) 654.
[10] E. Kohn, P. Gluche, M. Adamschik, Diamond Relat. Maters. 8 (1999) 934.
[11] F.J.H. Guillen, K. Janischowsky, J. Kusterer, W. Ebert, E. Kohn, Diamond Relat. Maters. 14 (2005) 411.
[12] D.M. Gruen, O.A. Shenderova, A.Ya. Vul' (Eds.), Synthesis, Properties and Applications of Ultrananocrystalline Diamond, NATO Science Series part II, vol. 192. (Springer, 2005).
[13] P.W. May, M. Hannaway, Mat. Res. Symp. Proc. PV-956 (2006) 0956–J09-31.
[14] S. Prawer, R.J. Nemanich, Phil. Trans. R. Soc. Lond. A 362 (2004) 2537.
[15] J.W. Ager III, W. Walukiewicz, M. McCluskey, M.A. Plano, M.I. Landstrass, Appl. Phys. Lett. 66 (1995) 616.
[16] F. Pruvost, E. Bustarret, A. Deneuville, Diamond Relat. Mater. 9 (2000) 295.
[17] Y.G. Wang, S.P. Lau, B.K. Tay, X.H. Zhang, J. Appl. Phys. 92 (2002) 7253.
[18] E. Gheeraert, P. Gonon, A. Deneuville, L. Abello, G. Lucazeau, Diamond Relat. Mater. 2 (1993) 742.
[19] P. Gonon, E. Gheeraert, A. Deneuville, L. Abello, G. Lucazeau, J. Appl. Phys. 78 (1995) 7059.
[20] R. Locher, J. Wagner, F. Fuchs, M. Maier, P. Gonon, P. Koidl, Diamond Relat. Mater. 4 (1995) 678.
[21] M. Bernard, A. Deneuville, P. Muret, Diamond Relat. Mater. 13 (2004) 282.
[22] M. Bernard, C. Baron, A. Deneuville Diamond Relat. Mater. 13 (2004) 896.
[23] J.P. Goss, P.R. Briddon, Phys. Rev. B 73 (2006) 085204.
[24] S. Prawer, K.W. Nugent, D.N. Jamieson, J.O. Orwa, L.A. Bursill, J.L. Peng, Chem. Phys. Lett. 332 (2000) 93.
[25] P.W. May, W.J. Ludlow, M. Hannaway, P.J. Heard, J.A. Smith, K.N. Rosser, Chem. Phys. Lett. 446 (2007) 103.
[26] D.W. Comerford, A. Cheesman, T.P.F. Carpenter, D.M.E. Davies, N.A. Fox, R.S. Sage, J.A. Smith, M.N.R. Ashfold, Yu. A. Mankelevich, J. Phys. Chem. A 110 (2006) 2868.
[27] A.C. Ferrari, J. Robertson, Phys. Rev. B 63 (2001) 121405.
[28] S.M. Leeds, T.J. Davis, P.W. May, C.D.O. Pickard, M.N.R. Ashfold, Diamond Relat. Mater. 7 (1998) 233.
[29] P.W. May, J.A. Smith, K.N. Rosser, Diamond Relat. Mater. (submitted for publication).